A Conic Model for Electrolyzer Scheduling – Online Companion

Enrica Raheli, Yannick Werner, and Jalal Kazempour
Department of Wind and Energy Systems, Technical University of Denmark, Kgs. Lyngby, Denmark
{enrah, yanwe, jalal}@dtu.dk

This Online Companion is a supplementary material to the paper *A Conic Model for Electrolyzer Scheduling*.

1. Modeling the hydrogen production curve: HYP-MISOC

In the following, we introduce model HYP-MISOC, an extension of model HYP-SOC with multiple segments. After presenting the mathematical model, we make some short comments about the exactness of the underlying relaxation. We then compare model HYP-MISOC to the other models with regards to solution accuracy and computational time based on the case studies introduced in the main paper.

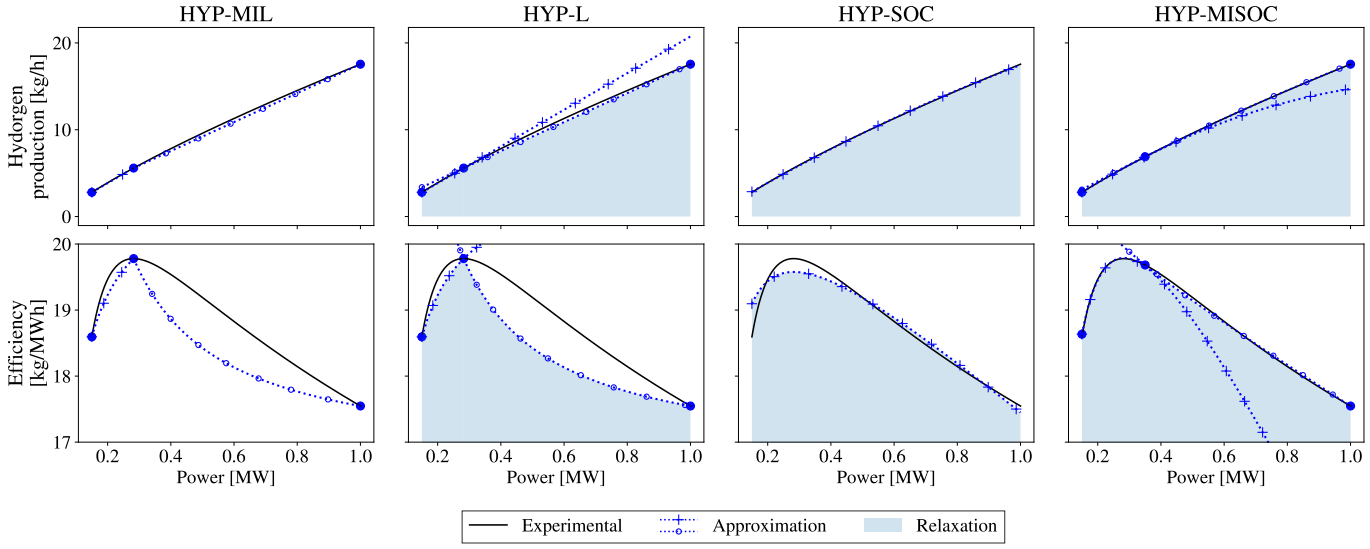

Fig. 7. Approximation (blue dashed) and relaxation (blue shaded) of the experimental non-convex (black) hydrogen production and efficiency curves using two segments (except HYP-SOC). The experimental hydrogen production and efficiency curves are taken from [14], based on [9], [10].

A. Mathematical model

Similar to the linear approaches HYP-MIL and HYP-L, HYP-SOC can be extended to account for multiple segments to obtain a more accurate representation of the experimental hydrogen production curve. This is achieved by performing multiple quadratic approximations and relaxing them into convex quadratic constraints:

$$h_t \leq \sum_{s\in\mathcal{S}} (A\widehat{p}^2_{s,t} + B\widehat{p}_{s,t} + C\widehat{z}_{s,t}), \qquad \forall t \in \mathcal{T}, \tag{10a}$$

$$\underline{P}_s \widehat{z}_{s,t} \leq \widehat{p}_{s,t} \leq \overline{P}_s \widehat{z}_{s,t}, \qquad \forall t \in \mathcal{T}, \quad \forall s \in \mathcal{S}, \tag{10b}$$

$$z^{\text{on}}_t = \sum_{s\in\mathcal{S}} \widehat{z}_{s,t}, \qquad \forall t \in \mathcal{T}, \tag{10c}$$

$$p_t = P^{\text{sb}} z^{\text{sb}}_t + \sum_{s\in\mathcal{S}} \widehat{p}_{s,t} \qquad \forall t \in \mathcal{T}, \tag{10d}$$

$$\widehat{z}_{s,t} \in \{0,1\}, \qquad \forall t \in \mathcal{T}, \quad \forall s \in \mathcal{S}. \tag{10e}$$

For the active segment, (10a) and (6) are equivalent when (10a) is binding at the optimal solution.

Model HYP-MISOC with two segments is shown along the other models in Figure 7. The two segments are chosen to best fit the experimental hydrogen production curve while ensuring a smooth fit including the hydrogen production corresponding

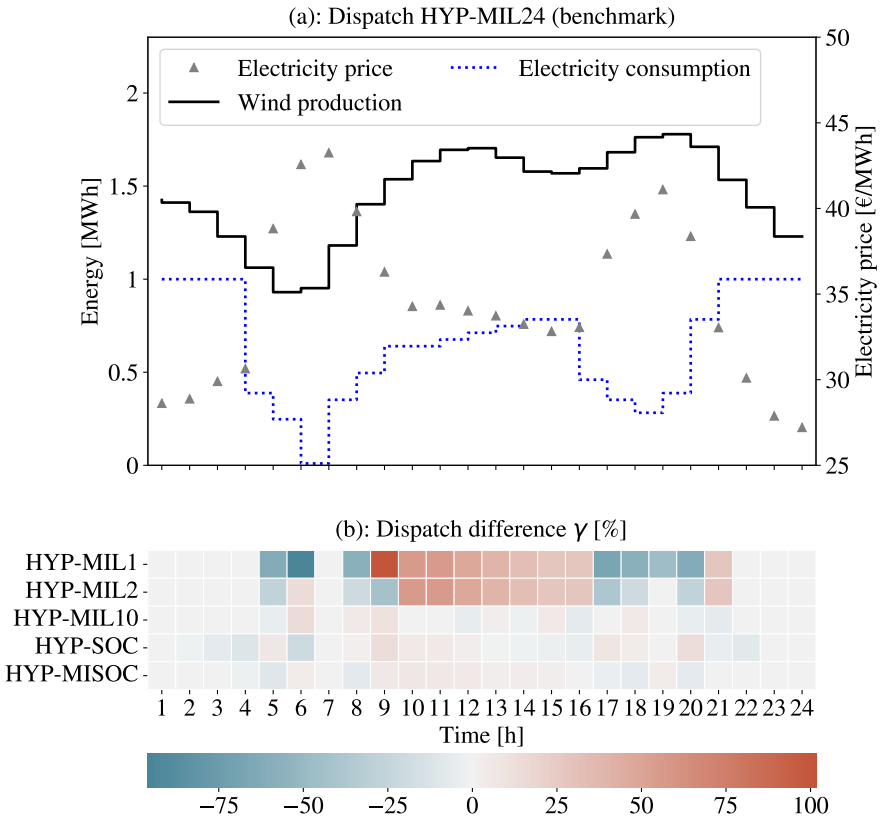

Fig. 8. (a): Optimal electrolyzer power consumption for the benchmark model HYP-MIL24 in an illustrative day. (b): Hourly relative difference γ_t of the optimal power consumption of the electrolyzer in the corresponding model with respect to that in the benchmark

to the minimum and maximum power consumption of the original curve. Since a comparatively high approximation accuracy is obtained with two segments only (see Figure 7), hereafter we assume that $|S| = 2$ for model HYP-MISOC. The set of variables for modeling the hydrogen production curve is $\mathbf{y}^{\text{MISOC}} = \{\widehat{p}_{s,t}, \widehat{z}_{s,t}\}$.

The optimal scheduling model for the hybrid power plant including hydrogen production curve HYP-MISOC is given by objective function (1a), the constraints for the hybrid power plant as a system (1b)–(1e), the operational states of the electrolyzer (2a)–(2f), and the hydrogen production curve (10a)–(10e). A summary and comparison to the other models is given in Table VII in Section 4 of this online companion.

B. Exactness

The solution accuracy of model HYP-MISOC depends on the exactness of relaxation (10a). Due to the binary variables in relaxation (10a) that indicate the active segment, the theorems and corresponding proofs given in the main paper do not directly apply. We run model HYP-MISOC for all the case studies presented in the main paper. The results are presented in the following section. Based on those results, we hypothesize that the theorems and proofs stated for model HYP-SOC in the main paper can be extended to model HYP-MISOC by taking the additional binary variables for the hydrogen production curve into account. We direct those derivations to future research.

C. Numerical study

We first compare model HYP-MISOC to the other models in terms of solution quality for an illustrative day. The dispatch for the HYP-MIL24 benchmark and the dispatch difference γ is shown in Figure 8. In comparison to the dispatch difference of model HYP-MIL2 of around 21%, model HYP-MISOC exhibits a significantly better performance, with an average error of around 3%. Compared to model HYP-SOC, model HYP-MISOC shows a slight increase of solution quality of around 2% based on the underlying HYP-MIL24 benchmark.

Table IV shows that ex-post comparison of the total annual profit, hydrogen production, and power sales of all models. We observe that the total annual profit for model HYP-MISOC is slightly higher than that of the HYP-MIL24 benchmark. This is due to an increase in hydrogen production, which is occasionally not profitable when approximating the hydrogen production curve with the HYP-MIL24 model. This indicates, that two quadratic approximations might reflect the experimental hydrogen production curve HYP-X even better than model HYP-MIL with 24 linear segments.

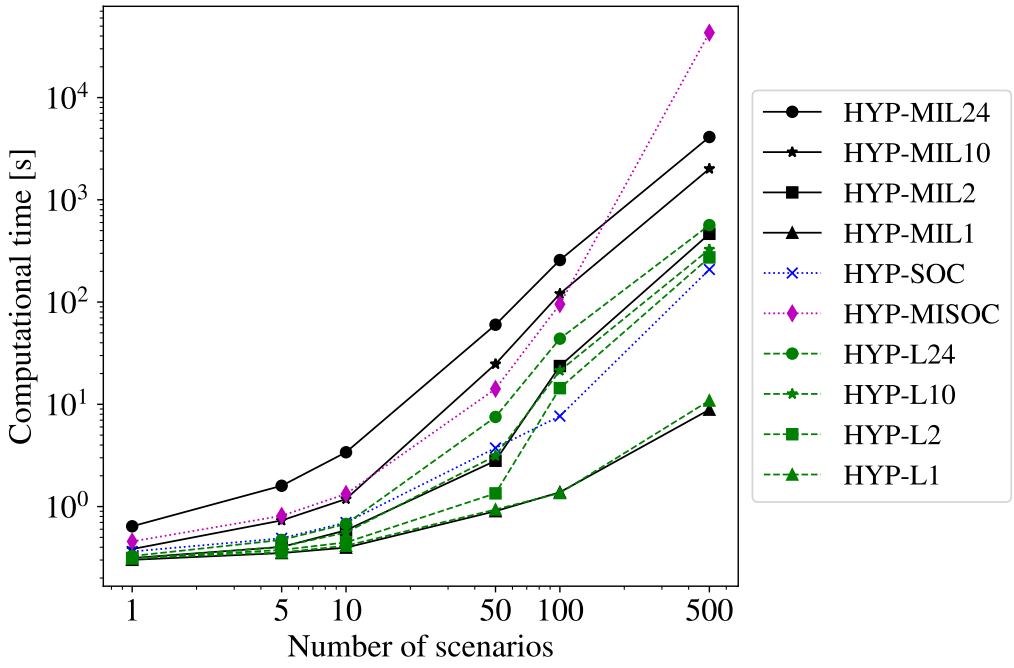

Fig. 9. Computational performance of different models for an increasing number of scenarios. Each data point represents the average computational time obtained from 100 repetitions, except for 500 scenarios, where only 10 repetitions (except HYP-MISOC) are used due to the increased computational time. For 500 scenarios, model HYP-MISOC is run a single time only.

TABLE IV
DIFFERENCE IN THE ANNUAL PROFIT, HYDROGEN PRODUCTION, AND POWER SALES COMPARED TO THE HYP-MIL24 BENCHMARK.

	Profit	Hydrogen production	Power sales
HYP-MIL24	-	-	-
HYP-MIL10	-0.003 %	-0.12 %	0.05 %
HYP-MIL2	-0.26 %	-7.06 %	3.66 %
HYP-MIL1	-0.63 %	-13.84 %	6.52 %
HYP-SOC	-0.01 %	-0.89 %	0.48 %
HYP-MISOC	0.001 %	0.19 %	-0.14 %

TABLE V
NUMBER OF VARIABLES AND CONSTRAINTS FOR MODELING THE HYDROGEN PRODUCTION CURVE AS A FUNCTION OF THE NUMBER OF SEGMENTS $|\mathcal{S}|$, TIME STEPS $|\mathcal{T}|$, AND SCENARIOS $|\Omega|$.

	# Variables		# Constraints	
	Binary	Continuous	LP/MILP	SOC/MISOC
HYP-MIL	$\|\mathcal{S}\|\|\mathcal{T}\|\|\Omega\|$	$\|\mathcal{S}\|\|\mathcal{T}\|\|\Omega\|$	$(2\|\mathcal{S}\|+3)\|\mathcal{T}\|\|\Omega\|$	0
HYP-L	0	$\|\mathcal{T}\|\|\Omega\|$	$(\|\mathcal{S}\|+3)\|\mathcal{T}\|\|\Omega\|$	0
HYP-SOC	0	$\|\mathcal{T}\|\|\Omega\|$	$3\|\mathcal{T}\|\|\Omega\|$	$\|\mathcal{T}\|\|\Omega\|$
HYP-MISOC	$2\|\mathcal{T}\|\|\Omega\|$	$2\|\mathcal{T}\|\|\Omega\|$	$6\|\mathcal{T}\|\|\Omega\|$	$2\|\mathcal{T}\|\|\Omega\|$

To evaluate the computational performance of model HYP-MISOC with respect to the size of the optimization model, we consider a two-stage stochastic version of HYP-MISOC, which is summarized in Table VII in Section 4 of this online companion. A comparison of variables and constraints required for HYP-MISOC and the other models is given in Table V. In contrast to model HYP-SOC, model HYP-MISOC requires additional binary variables for each segment. Recall that we assume that only two segments are needed to approximate the experimental hydrogen production curve well. The computational performance for the two-stage stochastic version of model HYP-MISOC compared to the other models for a different number of scenarios is given in Figure 9. Note that due to computational reasons, we run the HYP-MISOC model for 500 scenarios a single time only. We observe for 100 scenarios, that model HYP-MISOC solves around 20% faster than HYP-MIL10, which has roughly the same solution accuracy. For 500 scenarios, however, the computational time of HYP-MISOC increases significantly compared to all other model formulations. As shown in Table V, this is likely caused by a simultaneous increase of both binary variables and SOC constraints. We conclude that model HYP-MISOC achieves a very good solution accuracy but does not scale well with the problem size. Therefore, it may only be suitable for small scale problems when a high solution accuracy is desired.

2. REFORMULATION AS SECOND-ORDER CONE CONSTRAINT

Based on the underlying physics of the hydrogen production curve explained in Section I and shown in Figure 1 of the main paper, we assume that $A < 0$, such that constraints (7a) are convex quadratic inequality constraints [20]. In this case, they can be reformulated as second-order cone constraints as shown in the MOSEK Modeling Cookbook[6]. We repeat this reformulation for our specific case in scalar form here to ensure that this work is self-contained. The interested reader is referred to [20] and the MOSEK Modeling Cookbook for a more general overview on conic quadratic optimization.

[6]https://docs.mosek.com/modeling-cookbook/index.html

Constraints (7a) can be equivalently rewritten as

$$h_t + r_t - B\widetilde{p}_t - Cz_t^{\mathrm{on}} = 0, \qquad \forall\, t \in \mathcal{T}, \tag{11a}$$

$$-A\widetilde{p}_t^2 \leq r_t, \qquad \forall\, t \in \mathcal{T}. \tag{11b}$$

Since $A < 0$ by assumption, the epigraph (11b) is a convex set and there exists $R \in \mathbb{R}$, such that $-A = R^2$. Then (11b) can be reformulated as a rotated second-order cone constraint $(r_t, 1/2, R\widetilde{p}_t) \in \mathbb{Q}_{\mathrm{r}}^3$, where $\mathbb{Q}_{\mathrm{r}}^3$ is the set of 3-dimensional rotated second-order cones. An alternative representation based on the squared ℓ_2-norm is given by

$$\|R\widetilde{p}_t\|_2^2 \leq r_t, \quad \forall\, t \in \mathcal{T}. \tag{11c}$$

3. Selection of segments for model HYP-MIL and HYP-L

When the operation is not constrained by wind power availability or hydrogen demand, the optimal dispatch decision for models HYP-MIL and HYP-L always lies on one of the chosen linearization points. This is illustrated in Figure 3 in [14]. Consequently, the electrolyzer will usually operate in one of a small number of (discrete) operating points. Therefore, the selection of those linearization points for models HYP-MIL and HYP-L is important, as it impacts the solution quality and computational performance. Note that this is not the case for model HYP-SOC, which operates on the full (continuous) operational space of the approximation of the hydrogen production curve.

The selection of segments $\mathcal{S}$ for models HYP-MIL and HYP-L is done as follows: To capture the minimum and maximum hydrogen production as well as the one corresponding to the maximum efficiency, we partition the hydrogen production curve into two parts corresponding to the hydrogen production above (right side) and below (left side) the point corresponding to the maximum efficiency. For more than 2 segments, each side is further partitioned into equally distributed segments. The only exceptions are HYP-MIL1 and HYP-L1 which have only one linear segment between minimum and maximum hydrogen production points. The partition of segments on the left and right side is shown in Table VI. The interested reader is referred to [19], for instance, for a different choice of linearization points for the HYP-MIL.

TABLE VI
Partition of segments for models HYP-MIL and HYP-L.

Segments	Left side	Right side
24	4	20
10	2	8
2	1	1

4. Two-stage Stochastic Problem

In the following, we present the two-stage stochasting scheduling problem of the hybrid power plant for the different models of the hydrogen production curve. The first stage represents the day-ahead (DA) market and the second stage represents a generic real-time (RT) market. Table VII provides an overview on the two-stage stochastic optimal scheduling problem for the different hydrogen production curves, including model HYP-MISOC.

A. Objective function

The objective function aims at maximizing the expected profit of both day-ahead and balancing markets:

$$\max_{\mathbf{x}} \sum_{t\in\mathcal{T}} \Big(f_t\lambda_t + h_t\chi - z_t^{\mathrm{su}} K^{\mathrm{su}} \Big) + \sum_{\omega\in\Omega} \pi_\omega \sum_{t\in\mathcal{T}} \Big(\Delta_{t,\omega}^{\mathrm{up}} \lambda_t^{\mathrm{up}} - \Delta_{t,\omega}^{\mathrm{down}} \lambda_t^{\mathrm{down}} + (h_{t,\omega}^{\mathrm{RT}} - h_t)\chi - z_{t,\omega}^{\mathrm{su,RT}} K^{\mathrm{su}} \Big). \tag{12}$$

The non-negative variables $\Delta_{t,\omega}^{\mathrm{up}} \geq 0$ (up-regulation) and $\Delta_{t,\omega}^{\mathrm{down}} \geq 0$ (down-regulation) represent the real-time adjustment of power sold to the grid in time step t and scenario ω. These services are sold and bought, respectively, at prices $\lambda_t^{\mathrm{up}} < \lambda_t$ and $\lambda_t^{\mathrm{down}} > \lambda_t$. It is assumed that the hydrogen produced in real-time, $h_{t,\omega}^{\mathrm{RT}}$, is sold at the same constant price $\chi > 0$ as in the day-ahead market stage. Binary variable $z_{t,\omega}^{\mathrm{su,RT}}$ denotes the real-time startup of the electrolyzer.

B. Day-ahead constraints

The day-ahead constraints are the same as presented in Section II of the main paper, which are again summarized in Table VII in the online companion.

TABLE VII
SUMMARY OF DA AND RT CONSTRAINTS FOR THE FOUR DIFFERENT MODELS. THE OBJECTIVE FUNCTIONS FOR THE ONE-STAGE AND TWO-STAGE SCHEDULING PROBLEMS (1a) AND (12), RESPECTIVELY, ARE COMMON FOR ALL MODELS.

		HYP-MIL	HYP-L	HYP-SOC	HYP-MISOC
First-stage (DA)	Hybrid power plant	Power balance: (1b) Grid exchange: (1c) Hydrogen demand: (1d)–(1e)			
	Electrolyzer states	Mutual exclusiveness: (2a) Power consumption limits: (2b)–(2c) Startup and state binaries: (2d)–(2e), (2f)			
	Hydrogen production	(4a)–(4e)	(5a)–(5c)	(7a)–(7c)	(10a)–(10e)
Second-stage (RT)	Hybrid power plant	Power balance: (13a) Grid exchange: (13b) Hydrogen demand: (13c)–(13d)			
	Electrolyzer states	Mutual exclusiveness: (14a) Power consumption limits: (14b)–(14c) Startup and state binaries: (14d)–(14e), (14f)			
	Hydrogen production	(15a)–(15e)	(16a)–(16c)	(17a)–(17c)	(18a)–(18e)
	Model type	MILP	MILP	MISOCP	MISOCP

C. Real-time constraints

The real-time power balance of the hybrid power plant in real-time is given by:

$$(\mathrm{W}_t - \mathrm{W}^{\mathrm{RT}}_{t,\omega}) + (\Delta^{\mathrm{up}}_{t,\omega} - \Delta^{\mathrm{down}}_{t,\omega}) + (p^{\mathrm{RT}}_{t,\omega} - p_t) = 0, \quad \forall\, t \in \mathcal{T}, \quad \forall\, \omega \in \Omega, \tag{13a}$$

where $\mathrm{W}^{\mathrm{RT}}_{t,\omega}$ is the real-time wind power realization in scenario ω and W_t the mean over all scenarios in time step t. Variable $p^{\mathrm{RT}}_{t,\omega}$ is the real-time power consumption of the electrolyzer. To avoid buying electricity from the grid in real-time, the following constraint is added:

$$f_t - \Delta^{\mathrm{down}}_{t,\omega} \geq 0, \quad \forall\, t \in \mathcal{T}, \quad \forall\, \omega \in \Omega, \tag{13b}$$

The maximum hydrogen demand in real-time is limited by:

$$\sum_{t \in \mathcal{H}_n} h^{\mathrm{RT}}_{t,\omega} \leq D^{\max}_n, \quad \forall\, n \in \mathcal{N}, \quad \forall\, \omega \in \Omega, \tag{13c}$$

$$h^{\mathrm{RT}}_{t,\omega} \geq 0, \quad \forall\, t \in \mathcal{T}, \quad \forall\, \omega \in \Omega. \tag{13d}$$

Constraints (13d) ensure that the real-time hydrogen production is alaways non-negative.

The constraints that regulate the real-time operational states of the electrolyzer are derived by extending the corresponding day-ahead constraints (2a) – (2f) to each scenario ω:

$$z^{\mathrm{on,RT}}_{t,\omega} + z^{\mathrm{off,RT}}_{t,\omega} + z^{\mathrm{sb,RT}}_{t,\omega} = 1, \qquad \forall\, t \in \mathcal{T}, \qquad \forall\, \omega \in \Omega, \tag{14a}$$

$$p^{\mathrm{RT}}_{t,\omega} \leq P^{\max} z^{\mathrm{on,RT}}_{t,\omega} + P^{\mathrm{sb}} z^{\mathrm{sb,RT}}_{t,\omega}, \qquad \forall\, t \in \mathcal{T}, \qquad \forall\, \omega \in \Omega, \tag{14b}$$

$$p^{\mathrm{RT}}_{t,\omega} \geq P^{\min} z^{\mathrm{on,RT}}_{t,\omega} + P^{\mathrm{sb}} z^{\mathrm{sb,RT}}_{t,\omega}, \qquad \forall\, t \in \mathcal{T}, \qquad \forall\, \omega \in \Omega, \tag{14c}$$

$$z^{\mathrm{su,RT}}_{t,\omega} \geq z^{\mathrm{off,RT}}_{t-1,\omega} + z^{\mathrm{on,RT}}_{t,\omega} + z^{\mathrm{sb,RT}}_{t,\omega} - 1, \qquad \forall\, t \in \mathcal{T}\backslash 1, \qquad \forall\, \omega \in \Omega, \tag{14d}$$

$$z^{\mathrm{su,RT}}_{t=1,\omega} = 0, \qquad \forall\, \omega \in \Omega, \tag{14e}$$

$$z^{\mathrm{on,RT}}_{t,\omega}, z^{\mathrm{off,RT}}_{t,\omega}, z^{\mathrm{sb,RT}}_{t,\omega}, z^{\mathrm{su,RT}}_{t,\omega} \in \{0,1\}, \qquad \forall\, t \in \mathcal{T}, \qquad \forall\, \omega \in \Omega. \tag{14f}$$

D. Real-time hydrogen production curve

The constraints for the hydrogen production curve HYP-MIL in real-time are derived by extending the corresponding day-ahead constraints (4a) – (4e) to each scenario ω:

$$h^{\mathrm{RT}}_{t,\omega} = \sum_{s \in \mathcal{S}} (A_s \widehat{p}^{\mathrm{RT}}_{s,t,\omega} + B_s \widehat{z}^{\mathrm{RT}}_{s,t,\omega}), \qquad \forall\, t \in \mathcal{T}, \qquad \forall\, \omega \in \Omega, \tag{15a}$$

$$\underline{P}_s \widehat{z}^{\mathrm{RT}}_{s,t,\omega} \leq \widehat{p}^{\mathrm{RT}}_{s,t,\omega} \leq \overline{P}_s \widehat{z}^{\mathrm{RT}}_{s,t,\omega}, \qquad \forall\, s \in \mathcal{S}, \qquad \forall\, t \in \mathcal{T}, \qquad \forall\, \omega \in \Omega, \tag{15b}$$

$$\widetilde{z}^{\mathrm{on,RT}}_{t,\omega} = \sum_{s \in \mathcal{S}} \widehat{z}^{\mathrm{RT}}_{s,t,\omega}, \qquad \forall\, t \in \mathcal{T}, \qquad \forall\, \omega \in \Omega, \tag{15c}$$

$$p^{\mathrm{RT}}_{t,\omega} = P^{\mathrm{sb}} z^{\mathrm{sb,RT}}_{t,\omega} + \sum_{s \in \mathcal{S}} \widehat{p}^{\mathrm{RT}}_{s,t,\omega}, \qquad \forall\, t \in \mathcal{T}, \qquad \forall\, \omega \in \Omega, \tag{15d}$$

$$\widehat{z}^{\mathrm{RT}}_{s,t,\omega} \in \{0,1\}, \qquad \forall\, s \in \mathcal{S}, \qquad \forall\, t \in \mathcal{T}, \qquad \forall\, \omega \in \Omega. \tag{15e}$$

The constraints for the hydrogen production curve HYP-L in real-time are derived by extending the corresponding day-ahead constraints (5a) – (5c) to each scenario ω:

$$h^{\mathrm{RT}}_{t,\omega} \leq B_s \widetilde{p}^{\mathrm{RT}}_{t,\omega} + C_s z^{\mathrm{on,RT}}_{t,\omega}, \qquad \forall\, s \in \mathcal{S}, \qquad \forall\, t \in \mathcal{T}, \qquad \forall\, \omega \in \Omega, \tag{16a}$$

$$P^{\min} z^{\mathrm{on,RT}}_{t,\omega} \leq \widetilde{p}^{\mathrm{RT}}_{t,\omega} \leq P^{\max} z^{\mathrm{on,RT}}_{t,\omega}, \qquad \forall\, t \in \mathcal{T}, \qquad \forall\, \omega \in \Omega, \tag{16b}$$

$$p^{\mathrm{RT}}_{t,\omega} = \widetilde{p}^{\mathrm{RT}}_{t,\omega} + P^{\mathrm{sb}} z^{\mathrm{sb,RT}}_{t,\omega}, \qquad \forall\, t \in \mathcal{T}, \qquad \forall\, \omega \in \Omega. \tag{16c}$$

The constraints for the hydrogen production curve HYP-SOC in real-time are derived by extending the corresponding day-ahead constraints (7a) – (7c) to each scenario ω:

$$h^{\mathrm{RT}}_{t,\omega} \leq A(\widetilde{p}^{\mathrm{RT}}_{t,\omega})^2 + B\widetilde{p}^{\mathrm{RT}}_{t,\omega} + C z^{\mathrm{on,RT}}_{t,\omega}, \qquad \forall\, t \in \mathcal{T}, \qquad \forall\, \omega \in \Omega, \tag{17a}$$

$$P^{\min} z^{\mathrm{on,RT}}_{t,\omega} \leq \widetilde{p}^{\mathrm{RT}}_{t,\omega} \leq P^{\max} z^{\mathrm{on,RT}}_{t,\omega}, \qquad \forall\, t \in \mathcal{T}, \qquad \forall\, \omega \in \Omega, \tag{17b}$$

$$p^{\mathrm{RT}}_{t,\omega} = \widetilde{p}^{\mathrm{RT}}_{t,\omega} + P^{\mathrm{sb}} z^{\mathrm{sb,RT}}_{t,\omega}, \qquad \forall\, t \in \mathcal{T}, \qquad \forall\, \omega \in \Omega. \tag{17c}$$

The constraints for the hydrogen production curve HYP-MISOC in real-time are derived by extending the corresponding day-ahead constraints (10a) – (10d) to each scenario ω:

$$h^{\mathrm{RT}}_{t,\omega} \leq \sum_{s \in \mathcal{S}} (A(\widehat{p}^{\mathrm{RT}}_{s,t,\omega})^2 + B\widehat{p}^{\mathrm{RT}}_{s,t,\omega} + C\widehat{z}_{s,t,\omega}), \qquad \forall\, t \in \mathcal{T}, \qquad \forall\, \omega \in \Omega, \tag{18a}$$

$$\underline{P}_s \widehat{z}_{s,t,\omega} \leq \widehat{p}^{\mathrm{RT}}_{s,t,\omega} \leq \overline{P}_s \widehat{z}_{s,t,\omega}, \qquad \forall\, s \in \mathcal{S}, \qquad \forall\, t \in \mathcal{T}, \qquad \forall\, \omega \in \Omega, \tag{18b}$$

$$z^{\mathrm{on}}_{t,\omega} = \sum_{s \in \mathcal{S}} \widehat{z}_{s,t,\omega}, \qquad \forall\, t \in \mathcal{T}, \qquad \forall\, \omega \in \Omega, \tag{18c}$$

$$p^{\mathrm{RT}}_{t,\omega} = P^{\mathrm{sb}} z^{\mathrm{sb}}_t + \sum_{s \in \mathcal{S}} \widetilde{p}^{\mathrm{RT}}_{t,\omega}, \qquad \forall\, t \in \mathcal{T}, \qquad \forall\, \omega \in \Omega, \tag{18d}$$

$$\widehat{z}_{s,t,\omega} \in \{0,1\}, \qquad \forall\, s \in \mathcal{S}, \qquad \forall\, t \in \mathcal{T}, \qquad \forall\, \omega \in \Omega. \tag{18e}$$